Applied Catalysis B: Environmental 313 (2022) 121445

Contents lists available at ScienceDirect

Applied Catalysis B: Environmental

journal homepage: www.elsevier.com/locate/apcatb

Selective dehydrogenation of aqueous formic acid over multifunctional γ-Mo_2N catalysts at a temperature lower than 100 °C

Zhongliang Yu [a,b,*], Yanyan Yang [a], Song Yang [c], Jie Zheng [a], Xiaogang Hao [c], Guoqiang Wei [d], Hongcun Bai [e], Abuliti Abudula [f], Guoqing Guan [b,f,*]

[a] School of Chemistry and Environmental Science, Shangrao Normal University, Shangrao 334001, China
[b] Energy Conversion Engineering Laboratory, Institute of Regional Innovation (IRI), Hirosaki University, 3 Bunkyo-cho, Hirosaki, Aomori 036-8561, Japan
[c] Department of Chemical Engineering, Taiyuan University of Technology, Taiyuan 030024, China
[d] Institute of Biomass Engineering, Key Laboratory of Energy Plants Resource and Utilization, Ministry of Agriculture and Rural Affairs, South China Agricultural University, Guangzhou 510642, China
[e] State Key Laboratory of High-efficiency Utilization of Coal and Green Chemical Engineering, Ningxia University, Yinchuan 750021, China
[f] Graduate School of Science and Technology, Hirosaki University, 3 Bunkyo-cho, Hirosaki, Aomori 036-8561, Japan

ARTICLE INFO

Keywords:
Formic acid
Molybdenum nitride
Dehydration
Dehydrogenation
Hydrogen

ABSTRACT

Efficient and selective dehydrogenation of aqueous formic acid (FA) for hydrogen production with non-noble-metal-based heterogeneous catalysts remains a great challenge. Herein, complete dehydrogenation of aqueous FA with a concentration as high as 40 vol% achieved a gas production rate of 293.9 mL/$g_{cat.}$/h by using a biomass-derived multifunctional γ-Mo_2N catalyst synthesized with a facile pyrolysis process. No significant deactivation of catalysts was found during the 108 h-stability-test. Mechanism investigations indicate that the solvent H_2O could occupy the Brønsted acid sites to prevent FA dehydration. The dehydrogenation activity was significantly improved by the cooperation of K-containing sites, N-doped sites, and the γ-Mo_2N active sites, which could be responsible for the $HCOO^-$ intermediate generation and adsorption, H^+ adsorption, and H-C bond cleavage of the adsorbed $HCOO^-$, respectively. This study provided a novel strategy to improve the dehydrogenation performance of aqueous FA with non-noble-metal-based heterogeneous catalysts.

1. Introduction

Hydrogen is considering as an important green energy source to resolve the future energy and environmental crisis caused by the population growth, economic development, and rising living standards [1,2]. It can be the energy carrier of various intermittent energies such as solar, wind, and hydroelectric powers. However, efficient and safe storage and handling of hydrogen are still needed to be addressed for the successful incorporation of hydrogen energy into our energy infrastructure because of the disadvantages of H_2 arose from the low volumetric energy density (0.0108 MJ/L) and the easy-explosive property [3].

Several liquid compounds with mature synthesis processes, such as ammonia [4], formic acid (FA) [5,6], hydrazine [7] and methanol [8,9], have received considerable attention as chemical carriers for hydrogen storage and release. Especially, FA is one of the most promising hydrogen carriers with high volumetric (53 g/L) and gravimetric hydrogen density (4.4 wt%). Recent researches indicated that FA can be readily synthesized by either the CO_2 hydrogenation with renewable H_2 from solar and wind powers [10,11] and vice versa, it can be selectively dehydrogenated at ambient conditions (<100 °C, liquid phase) to produce high purity H_2 [15].

To date, majority of FA dehydrogenation in liquid phase has been performed in the presence of homogenous catalysts or noble metal based catalysts with the assistant of base additives (e.g., formate, amine, and triethylamine) and/or organic solvents [2,3,13,14]. However, by these ways, the following issues exist: 1) high cost with the precious metal-based catalysts; 2) separation difficulty because of the usage of homogenous catalysts or organic solvents, and the production of volatile organic compounds (VOCs) containing H_2; 3) high complexity of system

* Corresponding author at: School of Chemistry and Environmental Science, Shangrao Normal University, Shangrao 334001, China.
* Corresponding author at: Energy Conversion Engineering Laboratory, Institute of Regional Innovation (IRI), Hirosaki University, 3 Bunkyo-cho, Hirosaki, Aomori 036–8561, Japan.
E-mail addresses: yzh2401@126.com (Z. Yu), guan@hirosaki-u.ac.jp (G. Guan).

https://doi.org/10.1016/j.apcatb.2022.121445
Received 7 December 2021; Received in revised form 21 April 2022; Accepted 22 April 2022
Available online 26 April 2022
0926-3373/© 2022 Elsevier B.V. All rights reserved.

due to the requirement of solvents and additives. On the other hand, it is a practically favorable option to perform FA dehydrogenation under the aqueous condition since the commercial FA usually contains water. Thus, those catalysts without reasonable activity and stability in the presence of water could narrow their practical applicability for the FA dehydrogenation [15].

From the scientific and economic standpoints, it is appealing to develop non-noble metal based heterogeneous catalysts for the FA dehydrogenation without any organic solvents and additives to address all of the above issues. Although several precious metal-based catalysts have paved the way of FA dehydrogenation under mild conditions [16–18], the reports on the application of those non-precious ones are very limited [13], which mainly include highly dispersed CoN_x [19], cobalt single-atom and nanoparticle [20], cobalt@NC [21], $Mo_{1.98}C_{1.02}$ [22], and $Ti_3C_2T_x$ MXenes [23].

γ-Mo_2N with platinum-like properties has been intensively employed in many reactions [24–26]. Recently, we realized the selective dehydration of gaseous FA with the acidic bulk γ-Mo_2N [27], and achieved the selectivity transformation from dehydration to dehydrogenation by adjusting the acid-base sites [28]. Inspired by these results, we considered how to modulate the functional sites of γ-Mo_2N catalysts by elemental doping to realize the selective dehydrogenation of FA in liquid phase without any extra additives at a temperature lower than 100 °C. In this work, multifunctional C supported γ-Mo_2N catalyst was obtained by facile pyrolysis of a soybean-based protein as the natural K/N containing C precursor combining with ammonium molybdate. The catalyst performance was tested in a three-neck round-bottom flask filled with aqueous FA at low temperatures, and the resulting gas amount was measured by a graduated cylinder at first and then the gas compositions were analyzed by a gas chromatograph (GC). Meanwhile, a possible mechanism of selective dehydrogenation of aqueous FA was proposed.

2. Experimental

2.1. Catalyst preparation

The catalyst was typically synthesized as follows (the schematic diagram is shown in Fig. S1 in the supplement materials). Firstly, a certain amount of $(NH_4)_6Mo_7O_{24}$•4 H_2O (ammonium molybdate, AHM, Wako Chemicals, 99%) was dissolved by 20 mL of deionized water. Then, this aqueous solution was slowly added into 10.0 g of soybean-based protein powder (Wako Chemicals) under stirring to form a uniform paste. After ultrasonication treatment for 20 min, this paste was dried in 120 °C overnight. Finally, the dry paste was ground and then heated to 750 °C with a ramp rate of 10 °C/minute and held at this temperature for 2 h under Argon atmosphere (100 mL/min). As such, the C supported γ-Mo_2N catalyst doped with K/N was obtained. The fundamental analysis results of soybean-based protein powder from provider are summarized in Table S1. By air-TG, it was determined that the ash content of protein was 10.0 wt% (dry-basis), which was enriched into 24.2 wt% after the pyrolysis. Table S2 shows the ash composition of protein and obviously, it mainly consists of K (68.64 wt%). A notable pH value increase of the protein ash dispersed aqueous solution is shown in Fig. S2, indicating the presence of soluble solid bases. The K-containing compounds in catalyst can be roughly divided into soluble solid bases (such as K_2CO_3) and the insoluble species (such as potassium aluminosilicate) [29,30].

2.2. Activity test

The FA dehydrogenation reaction was performed in a three-neck round-bottom flask connected with a condenser and a graduated cylinder (Fig. S3). Firstly, 20 mL of aqueous FA solution and about 300 mg of catalyst were loaded into the flask. After the air inside the reactor was purged out by Ar gas, the flask was heated in an oil bath to the setting temperature and held stable at this temperature for 30 min. Thirdly, the volume of the evolved gas was measured by the graduated cylinder. The reflux temperature for condenser was set at 10 °C for all tests. After the reaction, the resulting gas was collected by a gas bag with Ar purging and analyzed using a gas chromatograph (GC) equipped with MolSieve 5A and Hayesep Q columns, and two TCD detectors (Agilent 7890A).

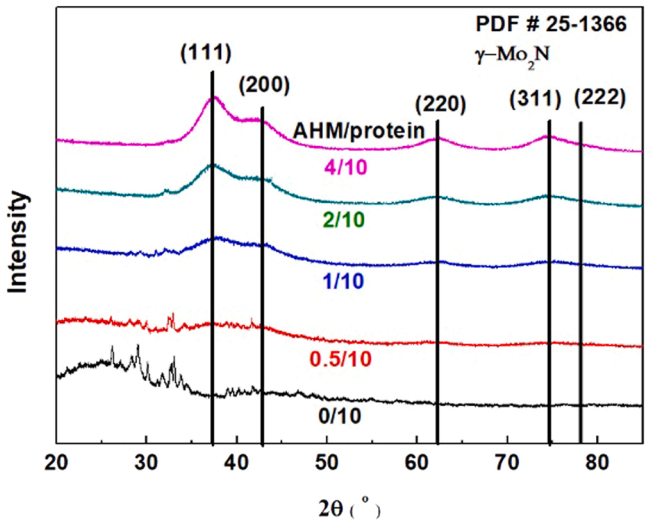

Fig. 1. XRD patterns of the soybean protein-derived C support and the as-prepared catalysts.

2.3. Catalyst characterizations

X-ray diffraction (XRD) pattern was measured by a powder X-ray diffractometer (Smartlab, Rigaku, Japan) using a CuKα radiation (λ = 0.15468 nm, 30 kV, 30 mA) within a scanning range of 10–90° at a scanning rate of 4°/min. The surface morphology and nanostructure of catalyst were observed by a Hitachi scanning electron microscope (SEM, SU8010, Japan) and a JEOL transmission electron microscope (TEM, JEM-2100 F). The high-angle annular dark-field scanning transmission electron microscopy (HAADF-STEM) images and element mapping were conducted by a Double Cs Corrector Transmission Electron Microscope (FEI ThemisZ). X-ray photoelectron spectroscopy (XPS) analysis was conducted using a Thermo Scientific ESCALAB 250Xi spectrometer with an Al Kα radiation (hυ = 1486.6 eV). N_2 adsorption (77 K) was applied to measure the Brunauer-Emmet-Teller (BET) surface area of catalysts using a Micromeritics ASAP 2020 C analyzer. Before measurement, the catalyst sample was vacuum-degassed at 200 °C for 10 h.

Element contents (C, H, N, and S) of catalysts were determined by an elemental analyzer (Vario EL Cube, Elementar Analysensysteme GmbH). Mo and K contents in the catalyst or the used FA solution was determined by an inductively coupled plasma optical emission spectroscopy (ICP-OES, Agilent ICP-OES 720). The ash content was analyzed by air-TG analysis (Shimadzu DTG-60 H).

Acid-base properties of catalyst were characterized by temperature-programmed desorption (TPD) with a BEL-CAT catalyst analyzer (BEL Inc) equipped with a TCD detector. Typically, ~0.0500 g of catalyst was loaded into a U-shape tube, which was then heated to 750 °C at a ramping rate of 10 °C/min and held at the final temperature for 2 h to activate the sample. After the activation, the sample was cooled to 100 °C in a stream of flowing He, and then saturated with NH_3 or CO_2 for 1 h. After the saturation, the U-shape tube was purged with He gas for 1 h to remove the weakly adsorbed species from catalyst surface. Finally, the TPD was performed by ramping the sample temperature at 10 °C/minute to 550 °C. The flowrate of NH_3 or CO_2 was set as 30 cm^3/min during the operation.

Pyridine-adsorbed infrared spectroscopy (Py-IR) was conducted by a Thermo scientific spectrometer (Nicolet 380). Prior to analysis, ~15 mg

Table 1
C, H, N, S, Mo, K contents and the surface areas of NK-C support and C supported catalyst.

Sample	N	C	H	S	Mo	K	surface area (m^2/g)
	(wt%)						
NK-C support	7.35	62.82	0.93	0.03	–	2.88	8.25
C supported γ-Mo_2N[a]	2.27 (0.91[b])	51.99	0.69	0.59	18.67 (20.03[c])	4.49	37.01

[a] corresponding to an AHM/protein ratio of 2/10 in the precursor
[b] N content incorporated into the carbon matrix
[c] γ-Mo_2N content determined by the Mo content.

of sample was pretreated at 550 °C for 1 h under a H_2/NH_3 atmosphere (v/v=1/1, 100 mL/min, balanced with Ar) for renitridation. After the pyridine injection at 40 °C with a saturation time of 30 min, the cell was heated and evacuated at 150 °C (or 250 °C) for 1 h. Thereafter, the catalyst was cooled down to 40 °C to record the IR spectra over 32 scans at a resolution of 4 cm^{-1}.

3. Results and discussion

3.1. Characteristics of prepared catalysts

To determine the phase composition, XRD spectra of catalysts and the support were analyzed. As shown in Fig. 1, the sharp reflexes at 2θ = 37.4°, 43.5°, 63.1°, 75.7°, and 79.7° are observed for all the Mo-based catalysts, corresponding to the (111), (200), (220), (311), and (222) facets of γ-Mo_2N (PDF #25–1366), respectively, which indicates that γ-Mo_2N has been successfully formed from the pyrolysis of soybean protein and ammonium molybdate mixture in Argon environment. Furthermore, with the increase of Mo addition amount in the initial solution, the peak intensity of γ-Mo_2N becomes more apparent, indicating the improvement of the crystallinity of γ-Mo_2N. In addition, it should be noted that the impurity peaks in the range of 25–35° are more obvious with the decrease of Mo addition amount in the initial solution, which should be attributed to the existence of ash in the original protein.

Table 1 compares C, N, H, S, Mo, and K contents of the C support and the C supported γ-Mo_2N catalyst. Beside C (62.82 wt%) as the main composition, it can be seen that the support also contains significant amounts of N (7.35 wt%) and K (2.88 wt%), indicating that the protein can be considered as not only the C source but also the N/K provider. The N, C, Mo, and K contents of the C supported γ-Mo_2N are 2.27 wt%, 51.99 wt%, 18.67 wt%, and 4.49 wt%, respectively. Assuming that one N atom combines two Mo atoms, the γ-Mo_2N content is determined to be 20.03 wt% based on the Mo content whereas 0.91 wt% of N is incorporated into the carbon matrix for the C supported γ-Mo_2N catalyst. The support should experience a shrink step during the pyrolysis of protein alone, which is indicated by the low BET surface area (8.25 m^2/g). While, the surface area of the C supported γ-Mo_2N is increased to 37.01 m^2/g with the addition of Mo, which could be due to the hole-opening effect of ammonium molybdate.

From the above results, it can be inferred that the γ-Mo_2N should be supported on a N/K co-doped carbon after the pyrolysis of protein with AHM. For clarity, these C supported γ-Mo_2N catalysts are denoted as γ-Mo_2N/*x*NK-C in the following, where *x* is the AHM/protein ratio. For example, γ-Mo_2N/*0.2*NK-C means the catalyst is obtained from an AHM/protein ratio of 2/10 in the precursor.

Fig. 2 and S4 show high-resolution TEM (HRTEM) and SEM images of the prepared γ-Mo_2N/*0.2*NK-C catalyst, respectively. One can see that this catalyst displays a non-porous surface (Fig. S4) and the γ-Mo_2N particles are homogeneously distributed over the C support (Fig. 2a) with an average particle size of 2.1 nm (Fig. 2b). The lattice fringes with the interplanar distances of 0.240 and 0.208 nm are clearly observed in the HRTEM image, which correspond to (111) and (200) planes of γ-Mo_2N, respectively (Fig. 2a). HAADF-STEM with energy-dispersive X-ray (EDX) mapping analysis was applied to further reveal the morphology and element distribution of Mo, N, K on the surface of catalyst (Fig. 3). In Fig. 3a, bright dots are uniformly dispersed on the support, and along with the EDX mapping of Mo (Fig. 3b), it could be concluded that those dots are γ-Mo_2N particles. From Fig. 3c-d, it can be inferred that the N/K are also uniformly distributed on the C support.

TPD and Py-IR analyses were applied to reveal the acidic and basic sites of catalyst (Fig. 4). The CO_2-TPD curve of γ-Mo_2N/*0.2*NK-C catalyst can be deconvoluted into three distinct and separated basic sites with the desorption temperatures at 174, 268, and 402 °C, respectively (Fig. 4a). While, the NH_3-TPD profile of γ-Mo_2N/*0.2*NK-C can be deconvoluted into two peaks with desorption temperatures at 168 °C and 213 °C, respectively (Fig. 4b). The CO_2/NH_3-TPD curves of γ-Mo_2N/*0.2*NK-C catalyst were also compared with those of NK-C support, and significant differences were observed (Fig. S5). Moreover, the Py-IR spectra reflect the existence of both Brønsted (B) and Lewis (L) acid sites on either the catalyst or the support surfaces (Fig. 4c and S6), which could be ascribed to the H-bonded species and the K dopant (Table 1), respectively. The acid density ratio of B/L for the γ-Mo_2N/*0.2*NK-C and NK-C support are calculated as 0.17 and 0.23, respectively.

The presence of Mo-N bond of γ-Mo_2N/*0.2*NK-C was also verified by the XPS spectra of Mo 3d, N 1 s, and K 2p (Fig. S7). The peak positions at 229.2 and 232.4 eV in Fig. S7a can be assigned to $Mo^{\delta+}$ $3d_{5/2}$ and $Mo^{\delta+}$ $3d_{3/2}$ of nitride, respectively, where $0 < \delta < 4$ [31,32]. While, the other two peaks at 232.5 and 235.6 eV are associated to Mo^{6+} $3d_{5/2}$ and Mo^{6+}

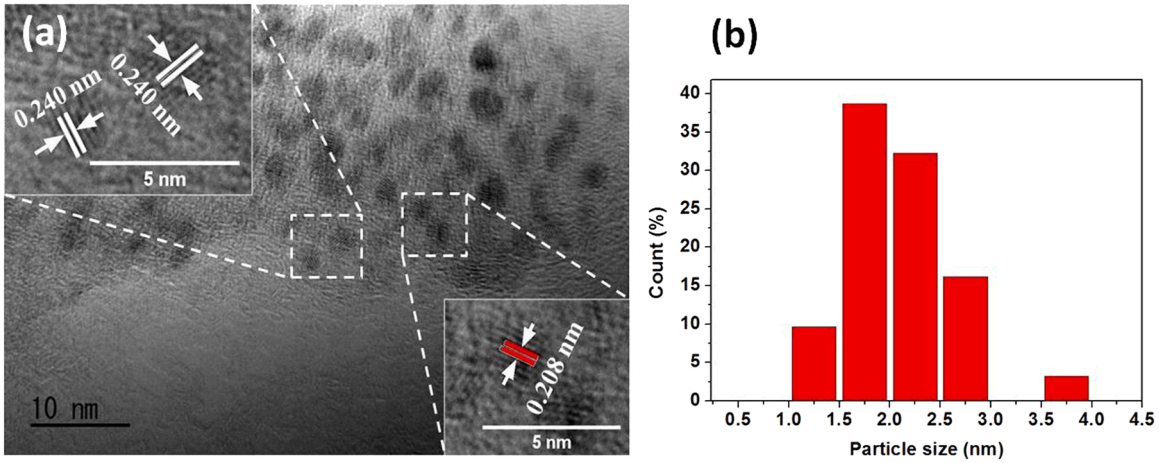

Fig. 2. HRTEM image (a) and size distribution histogram (b) of γ-Mo_2N/*0.2*NK-C catalyst.

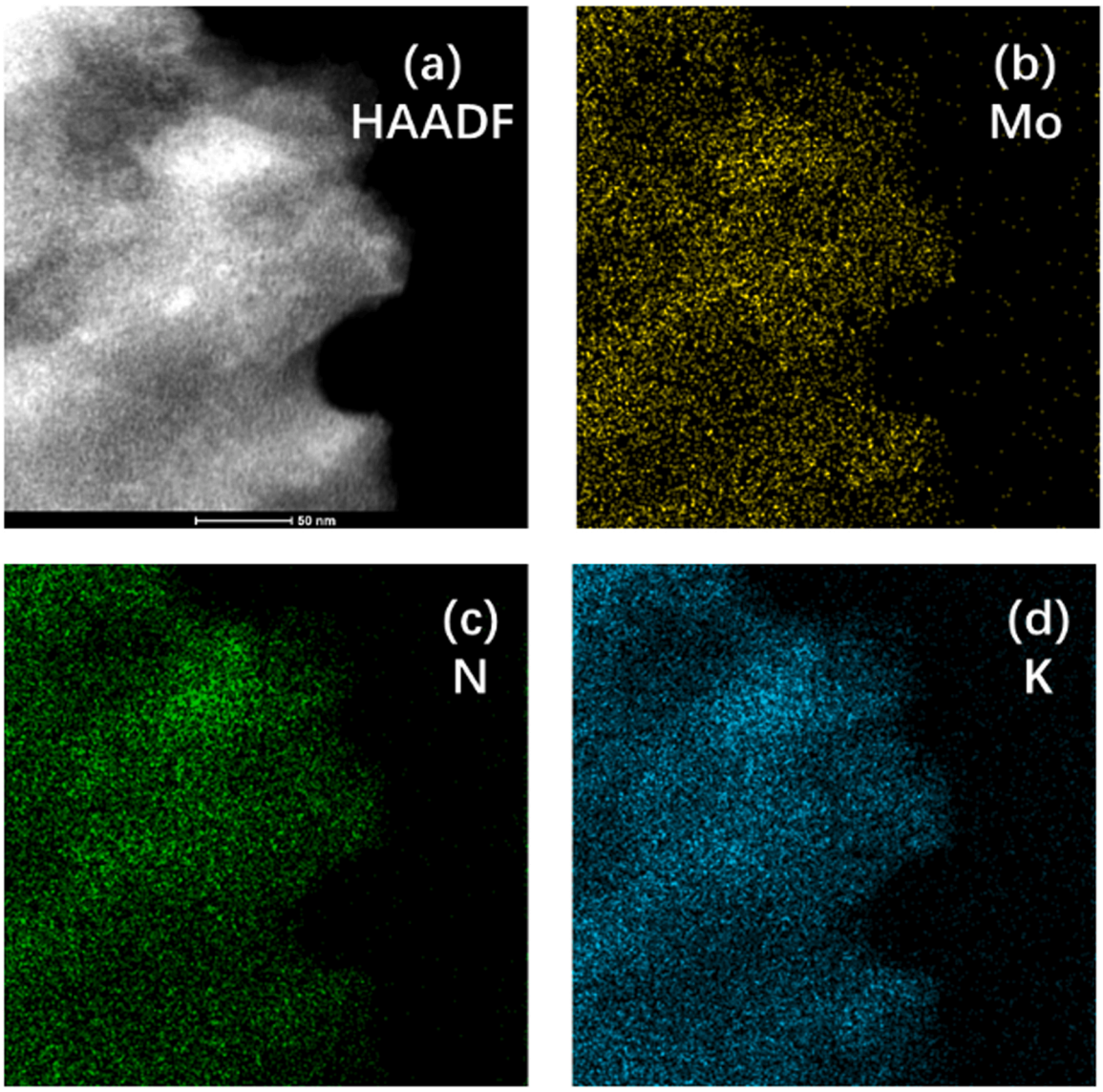

Fig. 3. HAADF-STEM mappings of the γ-Mo_2N/*0.2*NK-C catalyst: (a) HAADF, (b) Mo, (c) N, and (d) K.

$3d_{3/2}$, indicating the presence of MoO_3 on the surface of catalyst [31, 33]. Compared to the bulk and N-doped γ-Mo_2N/C catalysts [28], the peak position of $Mo^{\delta+}$ is shifted by 0.15 eV higher, suggesting that the electronic structure modulation occurs by the co-doping. The molybdenum oxides commonly existed on molybdenum nitrides or carbide due to the pyrophoricity nature of these kinds of materials in air. For XPS spectrum of N 1 s (Fig. S7b), the peaks at 395.8 and 398.1 eV can be assigned to the Mo 3p and the typical binding indicator of Mo-N bond, respectively. The other two peaks at 399.7 and 401.0 eV correspond to pyridinic-N and pyrrolic-N, respectively [33], but no apparent graphitic-N peak is observed. The presence of K^+ on the catalyst surface was also reflected by the main sharp line at 292.8 eV accompanied by a sharp satellite line at 295.6 eV (Fig. S7c) [34].

3.2. Catalytic performance

Fig. 5 indicates the effect of AHM to protein mass ratio in the precursor on the activity of the final obtained γ-Mo_2N/*x*NK-C catalysts. It can be seen from Fig. 5 that in the absence of Mo species, the N/K co-doped C support itself (0/10) shows no any notable activity. The catalytic activity increases with the increase of the AHM addition amount in the precursor when the AHM/protein mass ratio is lower than 2/10, suggesting that the γ-Mo_2N is involved in the rate-limiting step for the FA dehydrogenation in the liquid phase. The activity differences of these catalysts might be attributed to the varied γ-Mo_2N amounts as well as their structural differences in those parameters such as particle size and active site distribution. The non-increased activity by the catalyst synthesized with a higher AHM/protein weight ratio until 4/10 indicates that the excess molybdenum addition is unnecessary for the improvement of the activity. The generated H_2/CO_2 molar ratios are maintained at ca. 1/1 for all these catalysts in Fig. 5. Importantly, without any detectable CO, a FA dehydration product, is found in the gas product by GC, which should be benefit for the fuel cell applications by using the produced H_2 directly [15]. Hence, it is reasonable to conclude that the aqueous FA solution can be selectively dehydrogenated over the present N/K co-doped γ-Mo_2N catalysts.

Table 2 compares the performance of γ-Mo_2N/*0.2*NK-C catalyst with those of reported non-precious metal-based heterogeneous catalysts. Herein, although under a lower temperature and aqueous atmosphere, the performance of γ-Mo_2N/*0.2*NK-C was still comparable to those with other Co-based catalysts with organic solvent, and outperformed those reported catalysts except the $Ti_3C_2T_x$-250 when H_2O was used as the solvent. In addition, the FA concentration used in this work is much higher than those for other catalysts, which should be benefit for the

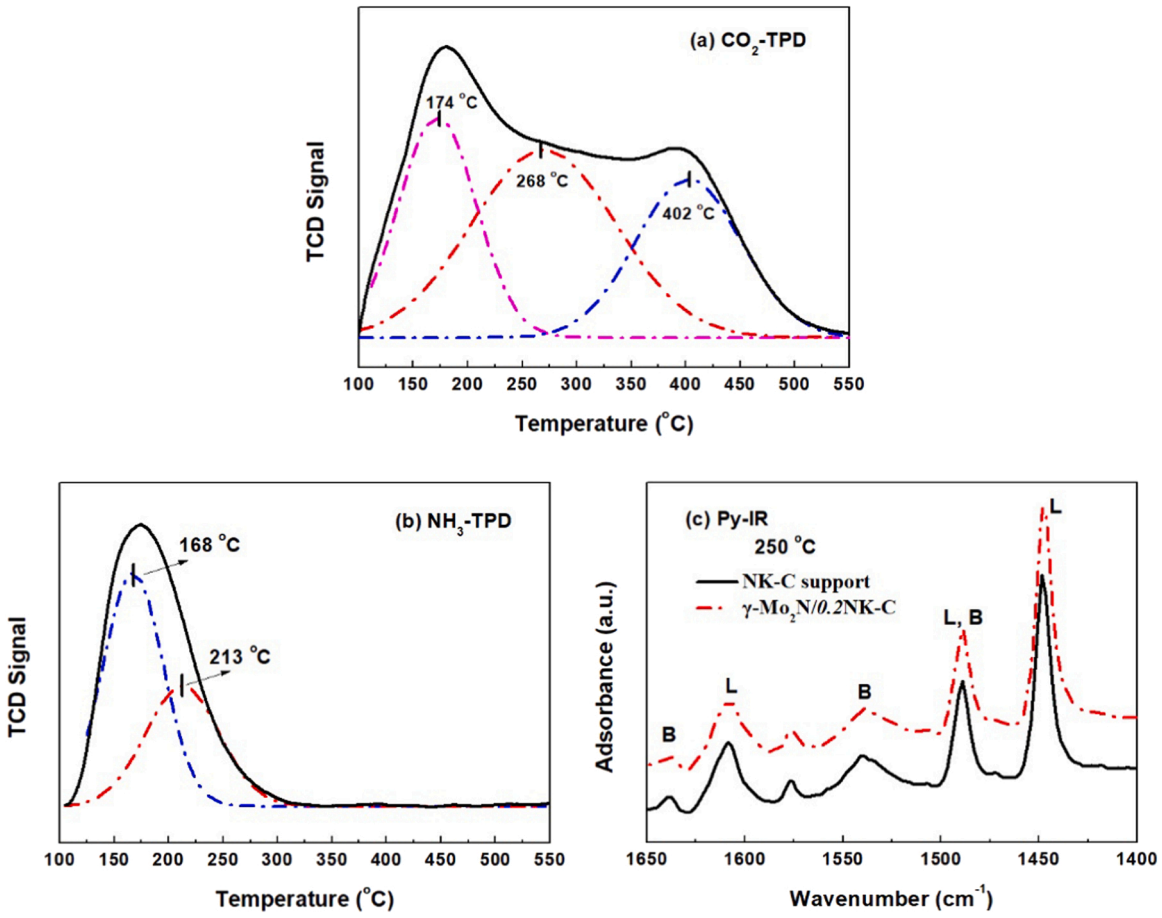

Fig. 4. CO_2- (a) and NH_3- (b) TPD curves of γ-Mo_2N/*0.2*NK-C catalyst, Py-IR profiles (c) of γ-Mo_2N/*0.2*NK-C catalyst and NK-C support.

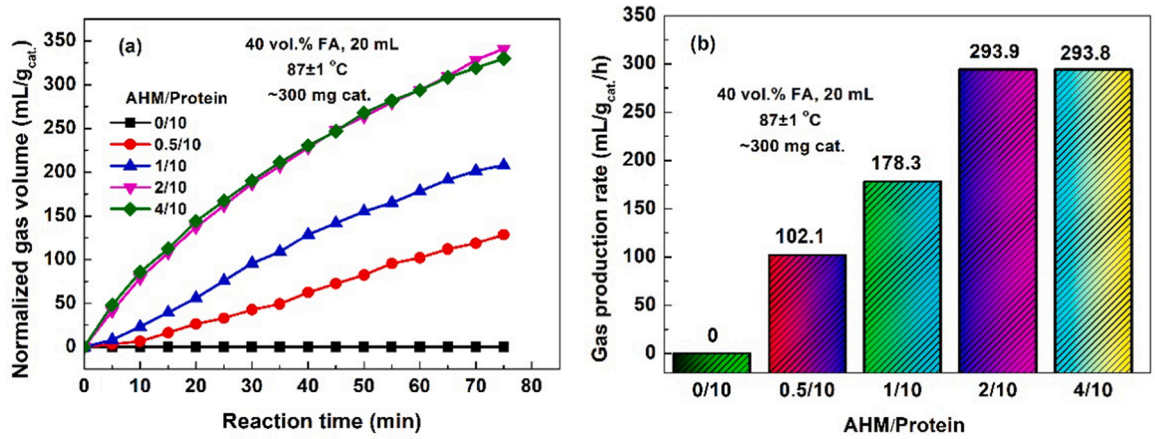

Fig. 5. Effect of mass ratio of AHM to protein in the precursor on the FA dehydrogenation with γ-Mo_2N/*x*NK-C catalysts: (a) normalized gas volume versus reaction time, and (b) gas production rate calculated with a reaction time of 60 min. All reactions were conducted at least twice with the fresh catalysts at the same condition.

practical hydrogen storage [35].

Long-term test (108 h) of aqueous FA (40 vol%) dehydrogenation over the γ-Mo_2N/*0.2*NK-C catalyst was conducted. Fig. 6 shows the accumulative gas volume change during the stability test. Continuously showing catalytic activity without apparent CO generation was observed during the 108 h test although the initial rate before ~5 h was faster than the later. Such a continuous activity of this catalyst was also found under a low FA concentration (7.7 vol%) environment (Fig. S8). These results suggest that this catalyst possessed stable activity in aqueous FA with different concentrations.

3.3. Mechanism investigation

Sufficient activity and selectivity are two important considerations for the liquid FA dehydrogenation with non-noble-metal-based heterogeneous catalysts at low temperatures. In this study, the catalyst was considered as the γ-Mo_2N nano-particles supported on N/K co-doped carbon with multifunctional sites, and the support itself was already proved to have no activity for FA dehydrogenation (Fig. 5). Thus, it is reasonable to consider the γ-Mo_2N as the crucial component of this catalyst. The roles of γ-Mo_2N active site and the N-doped site have been

Table 2
Comparison of liquid phase FA dehydrogenation over various non-noble metal-based heterogeneous catalysts.

Catalyst	Temperature (°C)	Solvent	FA concentration (mol/L)	Gas production rate (mL/g/h)	Reference
Co(1)/phen(7)/C	98	propylene carbonate	1.57	423.3	[19]
Co-N-C (SACs)	98	propylene carbonate	1.57	319.2	[20]
Co-N-C (NPs)	98	propylene carbonate	1.57	229.2	[20]
Co@NC-Gr2	95.5	o-xylene	1.24	124	[21]
Co(1)/phen(2)/C	95–100	H_2O	1.67	92.4	[19]
Co-N-C (SACs)	88	H_2O	1.57	167.9	[20]
Co-N-C (NPs)	88	H_2O	1.57	195.8	[20]
PF-$Mo_{1.98}C_{1.02}$	40–100	H_2O	1.25	790[a]	[22]
$Ti_3C_2T_x$-250	80	H_2O	0.26	365[b]	[23]
γ-Mo_2N/*0.2*NK-C	87	H_2O	10.39	293.9	This work

[a] 100 °C, sodium formate/FA molar ratio= 3/1
[b] 365 mmol/g/h, calculated within the initial 10 min

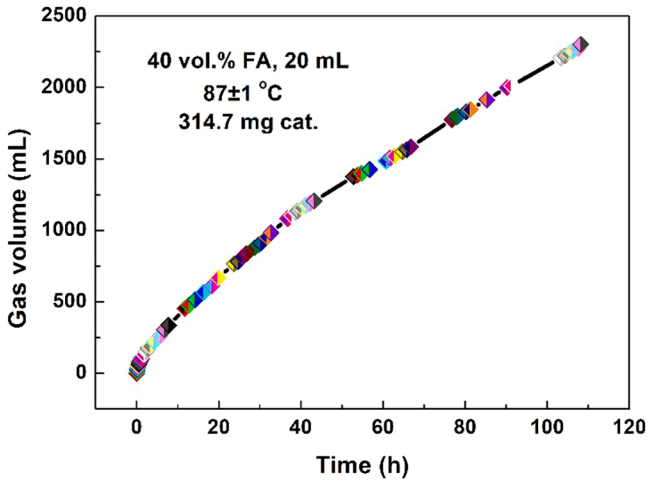

Fig. 6. Long-term experiment (108 h) of aqueous FA dehydrogenation over γ-Mo_2N/*0.2*NK-C catalyst.

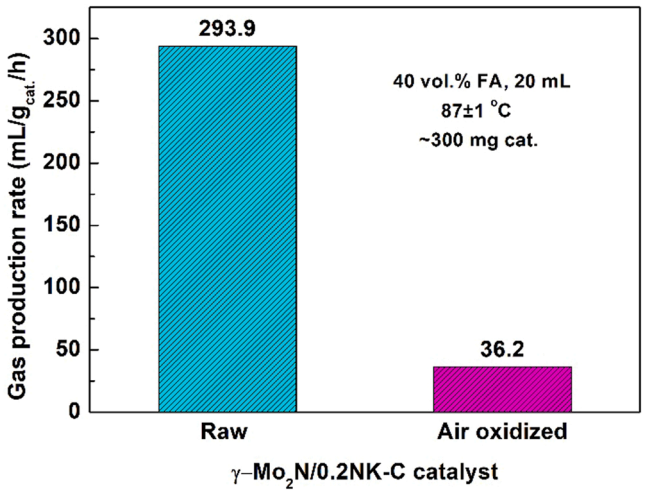

Fig. 7. Effect of air oxidation on the dehydrogenation activity of γ-Mo_2N/*0.2*NK-C catalyst.

Table 3
Mo and K contents of γ-Mo_2N/*0.2*NK-C catalyst and FA solution (40 vol%) after 108 h-stability test.

Sample	Mo	K	Unit
γ-Mo_2N/0.2NK-C	26.05	0.87	wt%
FA solution	2.5	557.0	mg/L

elucidated in our previous works [27,28], and thus the mechanism discussions here are mainly focused on the roles of K-containing sites and the Brønsted acid sites.

3.3.1. Roles of K-containing sites

The used catalyst and aqueous FA solution after the stability test were analyzed. Fig. S9 shows XRD pattern of the used γ-Mo_2N/*0.2*NK-C catalyst. Almost no change was found when compared to the XRD pattern of unused γ-Mo_2N/*0.2*NK-C catalyst, indicating that the γ-Mo_2N phase was stable in the aqueous FA system. The stability of γ-Mo_2N was also verified by that only a negligible Mo concentration of 2.5 mg/L was detected in the used FA solution, as shown in Table 3. However, significant K loss and K acquisition were also found as indicated in Table 3 for the used catalyst and the aqueous FA solution, respectively. Compared to the K content for the raw catalyst (Table 1), it is found that 80.6% of K on catalyst was leached by the FA solution after the stability test. The significant K leaching by FA solution was also reflected by the XPS spectrum of potassium (K 2p) (Fig. S10). Compared with the results shown in Fig. 4, the decrease in basicity and the increase in acidity after the reaction (Fig. S11) should be resulted from the leaching of solid bases and the FA adsorption on the used catalyst, respectively. The solid bases leaching by FA could produce potassium formate in the solution, which can be indicated by the K acquisition in solution (Table 3). Compared to the sole FA (weak acid) dissociation ($HCOOH \rightleftharpoons HCOO^- + H^+$), neutralization between solid bases with FA enhanced the production of formate ($HCOO^-$), which is an important intermediate of FA dehydrogenation [36]. The K^+ remained on the catalyst (19.4%) along with other cations impurities could act as the Lewis acid sites, accepting electrons donated from electronegative $HCOO^-$, forming HCOO-K adducts [37–39]. The N site could act as the Lewis base site [17,28], donating electrons to H^+ produced by FA dissociation. These electronic interactions could improve the adsorption of $HCOO^-$ and H^+ ions on catalyst surface for further decomposition.

3.3.2. Deactivation of γ-Mo_2N sites

The H-C bond of FA (HCOOH) could be broken by the nano-size γ-Mo_2N as that by the nano-palladium catalyst for FA dehydrogenation in liquid phase [17]. However, it is difficult to be cleaved by molybdenum oxides. In this work, the γ-Mo_2N was oxidized into MoO_3 (Fig. S12) by air oxidation at 400 °C (the support was almost not influenced by the oxidation). Fig. 7 compares the FA dehydrogenation activities of catalysts before and after air oxidation. It can be seen that the catalyst was remarkably deactivated after the oxidation (Fig. 7), and seriously megascopic dissolution was observed (Fig. S13), suggesting that the H-C bond breakage by γ-Mo_2N nano-particles could be the rate-limiting step of FA decomposition. Meanwhile, the N/K dopant might also act as electron donor/promotor to modulate the electronic structure of γ-Mo_2N [17,41], improving the H-C cleavage.

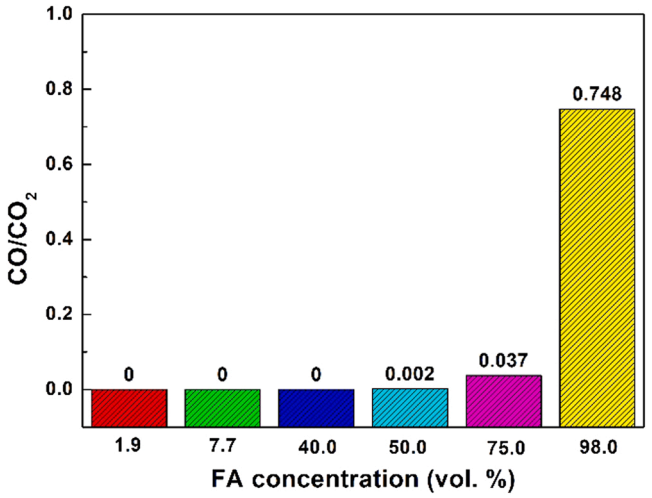

Fig. 8. Effect of FA concentration in the aqueous solution on the CO/CO_2 molar ratio of product gas with γ-Mo_2N/*0.2*NK-C catalyst. Reaction temperature: 87 ± 1 °C, catalyst amount: 50 mg.

3.3.3. *Effect of H_2O on the Brønsted acid sites*

The selectivity is another important factor for H_2 generation from FA. It is almost inevitable to completely avoid the formation of Brønsted acid sites during catalyst synthesis, which could donate H^+ to FA molecule, cleaving the C-OH bond for the dehydration pathway to generate CO [42–45]. In this study, since the Brønsted acid sites were also generated (Fig. 4c), it is reasonable to expect the CO generation during the FA decomposition. However, no notable CO was detected in the present aqueous FA decomposition system.

Although as a weak Brønsted base, H_2O shows higher basicity than FA, which suggests that H_2O could more likely to accept the H^+ donated by Brønsted acid site than that of FA in the aqueous system. To investigate the effect H_2O introduction, FA decomposition over γ-Mo_2N/*0.2*NK-C catalyst for a series of aqueous FA concentrations were also conducted. As shown in Fig. 8, the CO/CO_2 molar ratio was remained at zero when the FA concentrations were 1.9, 7.7, and 40 vol%, corresponding to 98.1, 92.3, and 60 vol% of the H_2O concentrations, respectively. When the FA concentration exceeded 50 vol%, a small amount of CO appeared with a CO/CO_2 molar ratio of 0.003. This ratio was further increased to 0.037 in the case with a FA concentration of 75 vol%. While, when the neat FA was used, the CO/CO_2 molar ratio was significantly increased to 0.748, indicating that both the dehydration and dehydrogenation pathways occurred apparently in the absence of H_2O. Fig. S14 compares the effect of aqueous FA concentration on CO_2/CO production rate. It can be seen that the dehydrogenation rate slowly increased with the increasing of FA concentration, while the dehydration rates kept at low levels in the presence of H_2O, but significantly increased to 247.0 mL/gcat./h for the neat FA. These two figures confirmed that the CO generation was effectively inhibited by the H_2O introduction to the reaction system, which could be due to the occupation of Brønsted acidic sites with H_2O molecules. The H_2O occupied Brønsted acidic sites could decrease its contact probability with FA molecules, inhibiting the C-OH bond cleavage for FA dehydration, thereby increasing the H_2 selectivity. Other possible explanation could be the changed reaction pathway of FA with the increased acidity (lowered pH) of the reaction solution with a high FA concentration [46].

3.3.4. *Proposed mechanism*

A possible mechanism of selective dehydrogenation of aqueous FA solution over γ-Mo_2N/*x*NK-C catalyst can be proposed as following (Fig. 9): 1) when the catalyst contacts with the aqueous FA solution, its Brønsted acid sites are occupied by H_2O molecules due to their comparatively stronger basicity than that of FA, preventing the C-OH bond cleavage for FA dehydration. While, some of FA molecules are

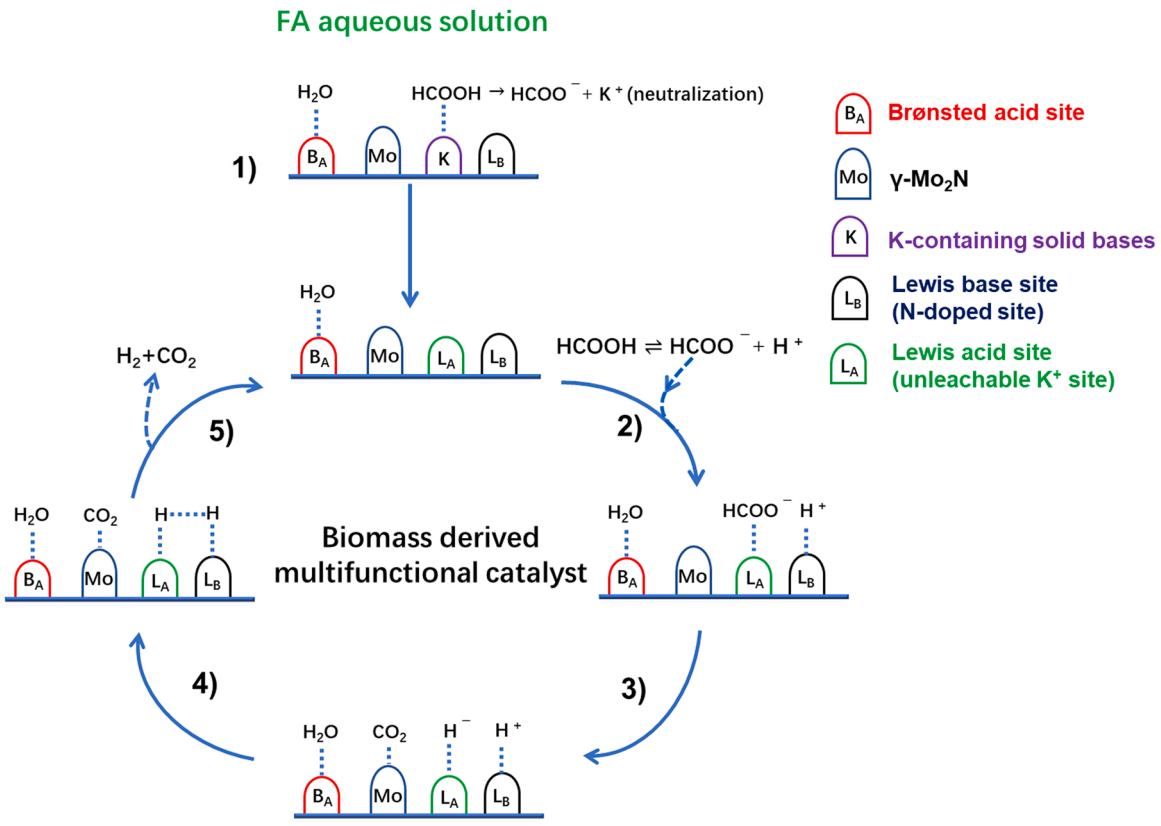

Fig. 9. Schematic diagram of a possible mechanism of selective dehydrogenation of aqueous FA solution over γ-Mo_2N/*x*NK-C catalyst.

neutralized by the leachable K-containing solid bases, producing $HCOO^-$ as the intermediate of FA dehydrogenation; 2) the unleachable K^+ dopants act as the Lewis acid sites, accepting electrons donated from $HCOO^-$, while the N dopants play the role of Lewis base sites, donating electrons to H^+ produced by FA dissociation; 3) the C-H bond cleavage of $HCOO^-$ (rate-limiting step) is then achieved by the "Pt-like" nano-Mo_2N sites, producing adsorbed CO_2 and H^-; 4) H^- on Lewis acid site combines the H^+ on Lewis base site to produce H_2; 5) the generated H_2 and CO_2 desorb from the catalyst surface to complete the dehydrogenation. The consumed $HCOO^-$ and H^+ in step 2) will be compensated by FA dissociation to start a new reaction cycle. As H_2O intensively exists in the aqueous solution reaction system, it can block the Brønsted acid site, and thus the aqueous FA is preferentially dehydrogenated into CO_2 and H_2.

4. Conclusions

A biomass-derived multifunctional C supported γ-Mo_2N catalyst was successfully synthesized by a facile pyrolysis process from soybean protein with ammonium molybdate. Complete FA dehydrogenation with a gas production rate of 293.9 mL/$g_{cat.}$/h was firstly realized at a temperature lower than 100 ℃ by using a high concentration aqueous FA (40 vol%) with this catalyst. A possible mechanism was proposed as follows: by adjusting the aqueous FA concentration, it was found that H_2O could occupy the Brønsted acid sites to prevent FA dehydration, thereby increasing the H_2 selectivity. Most of the K-containing solid bases on catalyst could be initially leached by aqueous FA solution, enhancing the formation of $HCOO^-$, an intermediate of FA dehydrogenation. The unleachable K^+ along with other cations impurities maintained on the catalyst could act as the Lewis acid sites to improve the $HCOO^-$ adsorption, while the N doped sites may play the role of Lewis base sites for H^+ ions adsorption. The H-C bond of adsorbed $HCOO^-$ is then cleaved by the γ-Mo_2N nanoparticles to produce CO_2 and H^-, and finally, H^- combines the H^+ to form H_2.

CRediT authorship contribution statement

Zhongliang Yu: Conceptualization, Investigation, Validation, Formal analysis, Writing – original draft, Writing – review & editing. **Yanyan Yang:** Investigation, Validation. **Song Yang:** Investigation, Validation. **Jie Zheng:** Investigation, Validation. **Xiaogang Hao:** Investigation, Validation. **Guoqiang Wei:** Investigation, Validation. **Hongcun Bai:** Investigation, Validation. **Abuliti Abudula:** Investigation, Validation. **Guoqing Guan**: Conceptualization, Resources, Visualization, Supervision,Writing – review & editing.

Declaration of Competing Interest

The authors declare that they have no known competing financial interests or personal relationships that could have appeared to influence the work reported in this paper.

Acknowledgements

This work is supported by National Natural Science Foundation of China (Nos. 22169017 and 51976226) and Foundation of State Key Laboratory of High-efficiency Utilization of Coal and Green Chemical Engineering (No. 2021-K61). Yu gratefully acknowledges the China Scholarship Council, China, and Hirosaki University, Japan.

Appendix A. Supporting information

Supplementary data associated with this article can be found in the online version at doi:10.1016/j.apcatb.2022.121445.

References

[1] K. Sordakis, C. Tang, L.K. Vogt, H. Junge, P.J. Dyson, M. Beller, G. Laurenczy, Homogeneous catalysis for sustainable hydrogen storage in formic acid and alcohols, Chem. Rev. 118 (2018) 372–433, https://doi.org/10.1021/acs.chemrev.7b00182.
[2] S. Enthaler, J. Von Langermann, T. Schmidt, Carbon dioxide and formic acid - the couple for environmental-friendly hydrogen storage? Energy Environ. Sci. 3 (2010) 1207–1217, https://doi.org/10.1039/b907569k.
[3] M. Grasemann, G. Laurenczy, Formic acid as a hydrogen source – recent developments and future trends, Energy Environ. Sci. 5 (2012) 8171–8181, https://doi.org/10.1039/C2EE21928J.
[4] A. Klerke, C.H. Christensen, J.K. Nørskov, T. Vegge, Ammonia for hydrogen storage: challenges and opportunities, J. Mater. Chem. 18 (2008) 2304–2310, https://doi.org/10.1039/B720020J.
[5] M. Navlani-García, K. Mori, D. Salinas-Torres, Y. Kuwahara, H. Yamashita, New approaches toward the hydrogen production from formic acid dehydrogenation over Pd-based heterogeneous catalysts, Front. Mater. 6 (2019) 1–18, https://doi.org/10.3389/fmats.2019.00044.
[6] H. Jeon, Y.-M. Chung, Hydrogen production from formic acid dehydrogenation over Pd/C catalysts: effect of metal and support properties on the catalytic performance, Appl. Catal. B Environ. 210 (2017) 212–222, https://doi.org/10.1016/J.APCATB.2017.03.070.
[7] R. Moury, G. Moussa, U.B. Demirci, J. Hannauer, S. Bernard, E. Petit, A. van der Lee, P. Miele, Hydrazine borane: synthesis, characterization, and application prospects in chemical hydrogen storage, Phys. Chem. Chem. Phys. 14 (2012) 1768–1777, https://doi.org/10.1039/C2CP23403C.
[8] K.I. Fujita, R. Kawahara, T. Aikawa, R. Yamaguchi, Hydrogen production from a methanol-water solution catalyzed by an anionic iridium complex bearing a functional bipyridonate ligand under weakly basic conditions, Angew. Chem. - Int. Ed. 54 (2015) 9057–9060, https://doi.org/10.1002/anie.201502194.
[9] L. Lin, W. Zhou, R. Gao, S. Yao, X. Zhang, W. Xu, S. Zheng, Z. Jiang, Q. Yu, Y.W. Li, C. Shi, X.D. Wen, D. Ma, Low-temperature hydrogen production from water and methanol using Pt/α-MoC catalysts, Nature 544 (2017) 80–83, https://doi.org/10.1038/nature21672.
[10] S. Moret, P.J. Dyson, G. Laurenczy, Direct synthesis of formic acid from carbon dioxide by hydrogenation in acidic media, Nat. Commun. 5 (2014) 4017.
[11] N. Onishi, R. Kanega, E. Fujita, Y. Himeda, Carbon dioxide hydrogenation and formic acid dehydrogenation catalyzed by iridium complexes bearing pyridyl-pyrazole ligands: effect of an electron-donating substituent on the pyrazole ring on the catalytic activity and durability, Adv. Synth. Catal. 361 (2019) 289–296, https://doi.org/10.1002/adsc.201801323.
[13] X. Wang, Q. Meng, L. Gao, Z. Jin, J. Ge, C. Liu, W. Xing, Recent progress in hydrogen production from formic acid decomposition, Int. J. Hydrog. Energy 43 (2018) 7055–7071, https://doi.org/10.1016/J.IJHYDENE.2018.02.146.
[14] T.C. Johnson, D.J. Morris, M. Wills, Hydrogen generation from formic acid and alcohols using homogeneous catalysts, Chem. Soc. Rev. 39 (2010) 81–88, https://doi.org/10.1039/b904495g.
[15] J. Eppinger, K.-W. Huang, Formic acid as a hydrogen energy carrier, ACS Energy Lett. 2 (2017) 188–195, https://doi.org/10.1021/acsenergylett.6b00574.
[16] K. Jiang, K. Xu, S. Zou, W. Cai, B-doped Pd catalyst: boosting room-temperature hydrogen production from formic acid–formate solutions, J. Am. Chem. Soc. 136 (2014) 4861–4864.
[17] Q.Y. Bi, J.D. Lin, Y.M. Liu, H.Y. He, F.Q. Huang, Y. Cao, Dehydrogenation of formic acid at room temperature: boosting palladium nanoparticle efficiency by coupling with pyridinic-nitrogen-doped carbon, Angew. Chem. - Int. Ed. 55 (2016) 11849–11853, https://doi.org/10.1002/anie.201605961.
[18] S. Jones, J. Qu, K. Tedsree, X.Q. Gong, S.C.E. Tsang, Prominent electronic and geometric modifications of palladium nanoparticles by polymer stabilizers for hydrogen production under ambient conditions, Angew. Chem. - Int. Ed. 51 (2012) 11275–11278, https://doi.org/10.1002/anie.201206035.
[19] C. Tang, A.-E. Surkus, F. Chen, M.-M. Pohl, G. Agostini, M. Schneider, H. Junge, M. Beller, A stable nano-cobalt catalyst for selective dehydrogenation of formic acid with highly dispersed conx active sites, Angew. Chem. Int. Ed. 56 (2017) 16616–16620, https://doi.org/10.1002/anie.201710766.
[20] X. Li, A.E. Surkus, J. Rabeah, M. Anwar, S. Dastgir, H. Junge, A. Brückner, M. Beller, Cobalt single-atom catalysts with high stability for selective dehydrogenation of formic acid, Angew. Chem. - Int. Ed. 59 (2020) 15849–15854, https://doi.org/10.1002/anie.202004125.
[21] A.N. Chernov, T.V. Astrakova, V.I. Sobolev, K.Y. Koltunov, Liquid versus gas phase dehydrogenation of formic acid over Co@N-doped carbon materials. The role of single atomic sites, Mol. Catal. 504 (2021), 111457, https://doi.org/10.1016/j.mcat.2021.111457.
[22] C. Lv, P. Lou, C. Shi, R. Wang, Y. Fu, L. Gao, S. Wang, Y. Li, C. Zhang, Efficient hydrogen productionviasunlight-driven thermal formic acid decomposition over a porous film of molybdenum carbide, J. Mater. Chem. A. 9 (2021) 22481–22488, https://doi.org/10.1039/d1ta06059g.
[23] T. Hou, Q. Luo, Q. Li, H. Zu, P. Cui, S. Chen, Y. Lin, J. Chen, X. Zheng, W. Zhu, S. Liang, J. Yang, L. Wang, Modulating oxygen coverage of $Ti_3C_2T_x$ MXenes to boost catalytic activity for HCOOH dehydrogenation, Nat. Commun. 11 (2020) 1–11, https://doi.org/10.1038/s41467-020-18091-7.
[24] J.A. Schaidle, L.T. Thompson, Fischer-Tropsch synthesis over early transition metal carbides and nitrides: CO activation and chain growth, J. Catal. 329 (2015) 325–334, https://doi.org/10.1016/j.jcat.2015.05.020.
[25] S. Boullosa-Eiras, R. Lødeng, H. Bergem, M. Stöcker, L. Hannevold, E.A. Blekkan, Catalytic hydrodeoxygenation (HDO) of phenol over supported molybdenum

carbide, nitride, phosphide and oxide catalysts, Catal. Today 223 (2014) 44–53, https://doi.org/10.1016/j.cattod.2013.09.044.
[26] M. Nagai, Y. Goto, A. Irisawa, S. Omi, Catalytic activity and surface properties of nitrided molybdena-alumina for carbazole hydrodenitrogenation, J. Catal. 191 (2000) 128–137, https://doi.org/10.1006/jcat.1999.2788.
[27] Z. Yu, A. Yoshida, J. Shi, T. Wang, S. Yang, Q. Ye, X. Hao, A. Abudula, Y. Fang, G. Guan, Formic acid as a Bio-CO carrier: selective dehydration with γ-Mo_2N Catalysts at low temperatures, ACS Sustain. Chem. Eng. 8 (2020) 13956–13963, https://doi.org/10.1021/acssuschemeng.0c03269.
[28] Z. Yu, X. An, I. Kurnia, A. Yoshida, Y. Yang, X. Hao, A. Abudula, Y. Fang, G. Guan, Full spectrum decomposition of formic acid over γ-Mo_2N-based catalysts: from dehydration to dehydrogenation, ACS Catal. 10 (2020) 5353–5361, https://doi.org/10.1021/acscatal.0c00752.
[29] S.V. Vassilev, C.G. Vassileva, Water-soluble fractions of biomass and biomass ash and their significance for biofuel application, Energy Fuels 33 (2019) 2763–2777, https://doi.org/10.1021/acs.energyfuels.9b00081.
[30] J. Werkelin, B.J. Skrifvars, M. Zevenhoven, B. Holmbom, M. Hupa, Chemical forms of ash-forming elements in woody biomass fuels, Fuel 89 (2010) 481–493, https://doi.org/10.1016/j.fuel.2009.09.005.
[31] Z.B.Z. Wei, P. Grange, B. Delmon, XPS and XRD studies of fresh and sulfided Mo_2N, Appl. Surf. Sci. 135 (1998) 107–114, https://doi.org/10.1016/S0169-4332(98)00267-0.
[32] J. Liu, S. Tang, Y. Lu, G. Cai, S. Liang, W. Wang, X. Chen, Synthesis of Mo_2N nanolayer coated MoO_2 hollow nanostructures as high-performance anode materials for lithium-ion batteries, Energy Environ. Sci. 6 (2013) 2691, https://doi.org/10.1039/c3ee41006d.
[33] Y.J. Song, Z.Y. Yuan, One-pot synthesis of Mo_2N/NC catalysts with enhanced electrocatalytic activity for hydrogen evolution reaction, Electrochim. Acta 246 (2017) 536–543, https://doi.org/10.1016/j.electacta.2017.06.086.
[34] A. Miyakoshi, A. Ueno, M. Ichikawa, XPS and TPD characterization of manganese-substituted iron-potassium oxide catalysts which are selective for dehydrogenation of ethylbenzene into styrene, Appl. Catal. A Gen. 219 (2001) 249–258, https://doi.org/10.1016/S0926-860X(01)00697-4.
[35] Q. Liu, X. Yang, Y. Huang, S. Xu, X. Su, X. Pan, J. Xu, A. Wang, C. Liang, X. Wang, T. Zhang, A. Schiff, base modified gold catalyst for green and efficient H_2 production from formic acid, Energy Environ. Sci. 8 (2015) 3204–3207, https://doi.org/10.1039/c5ee02506k.
[36] I. Kovács, J. Kiss, Z. Kónya, The potassium-induced decomposition pathway of HCOOH on Rh(111), Catalysts 10 (2020), https://doi.org/10.3390/catal10060675.
[37] L. Jia, D.A. Bulushev, J.R.H. Ross, Formic acid decomposition over palladium based catalysts doped by potassium carbonate, Catal. Today 259 (2016) 453–459, https://doi.org/10.1016/j.cattod.2015.04.008.
[38] D.A. Bulushev, M. Zacharska, S. Beloshapkin, Y. Guo, I. Yuranov, Catalytic properties of PdZn/ZnO in formic acid decomposition for hydrogen production, Appl. Catal. A Gen. 561 (2018) 96–103, https://doi.org/10.1016/J.APCATA.2018.05.025.
[39] D.A. Bulushev, M. Zacharska, Y. Guo, S. Beloshapkin, A. Simakov, CO-free hydrogen production from decomposition of formic acid over Au/Al_2O_3 catalysts doped with potassium ions, Catal. Commun. 92 (2017) 86–89, https://doi.org/10.1016/j.catcom.2017.01.011.
[41] D. Moszyński, R. Jedrzejewski, J. Ziebro, W. Arabczyk, Surface and catalytic properties of potassium-modified cobalt molybdenum catalysts for ammonia synthesis, Appl. Surf. Sci. 256 (2010) 5581–5584, https://doi.org/10.1016/j.apsusc.2009.12.150.
[42] E.M. Sadovskaya, Y.A. Chesalov, V.B. Goncharov, V.I. Sobolev, T. V. Andrushkevich, Formic acid decomposition over V-Ti oxide catalyst: Mechanism and kinetics, Mol. Catal. 430 (2017) 54–62, https://doi.org/10.1016/J.MOLCATA.2016.12.010.
[43] G.Y. Popova, Y.A. Chesalov, E.M. Sadovskaya, T.V. Andrushkevich, Effect of water on decomposition of formic acid over V–Ti oxide catalyst: Kinetic and in situ FTIR study, J. Mol. Catal. A Chem. 357 (2012) 148–153, https://doi.org/10.1016/J.MOLCATA.2012.02.005.
[44] M. Ai, Activities for the decomposition of formic acid and the acid-base properties of metal oxide catalysts, J. Catal. 50 (1977) 291–300, https://doi.org/10.1016/0021-9517(77)90038-0.
[45] J.M. Trillo, G. Munuera, J.M. Criado, Catalytic decomposition of formic acid on metal oxides, Catal. Rev. 7 (1972) 51–86, https://doi.org/10.1080/01614947208064710.
[46] J.S.J. Ferrer, E. Couallier, M. Rakib, G. Durand, Electrochemical determination of acidity level and dissociation of formic acid/water mixtures as solvent, Electrochim. Acta 52 (2007) 5773–5780, https://doi.org/10.1016/j.electacta.2007.02.058.